CEAS-GNC-2024-082

EuroGNC Navigation Guidance Control CEAS Bristol, UK June 11th-13th 2024
University of BRISTOL ROYAL AERONAUTICAL SOCIETY AIAA

Flight Testing Air Data Sensor Failure Handling with Hybrid Nonlinear Dynamic Inversion

Daniel Milz Research Associate, German Aerospace Center (DLR), Institute of System Dynamics and Control, 82234, Weßling, Germany. daniel.milz@dlr.de

Marc May Research Associate, German Aerospace Center (DLR), Institute of System Dynamics and Control, 82234, Weßling, Germany. marc.may@dlr.de

Gertjan Looye Head of Department, German Aerospace Center (DLR), Institute of System Dynamics and Control, 82234, Weßling, Germany. gertjan.looye@dlr.de

ABSTRACT

Loss of one or more air data signals to the flight control laws typically results in activation of backup modes. These reduce functionality and work solely with inertial sensors. Since the failure situation is already a significant stress for the flight crew, this reduction of supporting control functionality comes at an awkward moment. This work shows how a combination of classical and so-called sensory nonlinear dynamic inversion can be used to maintain more or less the same handling characteristics in case of partial or even complete loss of air data. Under nominal conditions, hybrid NDI uses a complementary filter to combine NDI and sensory NDI. In case of failure, it is possible to degrade to a control law based purely on sensory NDI, which is predominantly inertial sensor dependent. This paper describes the application of the proposed modification to a CS-25 class aircraft, as well as the validation of its intended features in flight tests.

Keywords: Flight Control; Flight Test; Dynamic Inversion; Air Data Sensor; Sensor Failure; Fault-Tolerant Control

Nomenclature

$\boldsymbol{\omega}$	=	Angular rates
V_a	=	air speed
α	=	angle of attack
β	=	sideslip angle
$\boldsymbol{I}$	=	moment of inertia
$\bar{q}$	=	dynamic pressure
S	=	aero. reference area
$\bar{c}$	=	mean aero. chord length
$\frac{b}{2}$	=	half span-width
$\boldsymbol{C}_\delta$	=	control effectiveness
C_l	=	aero. roll moment coefficient
C_m	=	aero. pitch moment coefficient
C_n	=	aero. yaw moment coefficient
x	=	state vector
u	=	input vector
y	=	output vector
$f(x)$	=	internal dynamics
$G(x)$	=	input dynamics
ν	=	virtual control input
$\hat{}$	=	Estimation or measurement of quantity

1 Introduction

The air data sensor system is a particularly critical component in modern aircraft for two main reasons: Air data is crucial for both the flight control system (FCS) and the pilot, as it enables them to control and assess the current state of the aircraft. Additionally, air data sensors are often fragile, consisting primarily of mechanical components that can be easily disrupted by factors such as icing or sticking. In the event of one or more air data sensor failures, many modern aircraft will degrade their level of automation and delegate more responsibility to the pilot [1]. The degraded control law changes the handling behavior of the aircraft, requiring pilots to adapt and potentially increasing their workload even more [2]. Current research on air data sensor failures focuses mainly on detecting and identifying failures [3], reconstructing erroneous measurements [4], or deploying robust or adaptive control laws in case of failure [5]. However, the first approaches rely on the quality of the sensor value reconstruction. If successful, this may be the superior solution to the overall problem of air data sensor failure. However, this is still an ongoing research area, and there has yet to be a production-ready and certifiable solution. The latter approach is the prevailing method for dealing with air data sensor failure, mostly by degrading to a reduced but more robust law. However, this leads to the previously mentioned degradation and changes in handling behavior.

Current developments in flight control research focus among others on inversion-based methods. These methods offer a close-to-physics approach while modularizing flight control functions and properties, allowing for the automation of multiple aircraft control tasks via command filters [6]. These include rate-command-attitude-hold filters, reference models specifying the dynamic behavior of the aircraft, or dynamic envelope protections. Nonlinear dynamic inversion (NDI) and Feedback Linearization are the common precursors of current developments in inversion-based control. These methods have in common that they achieve an uncoupling of the aircraft's dynamics. However, to cancel the nonlinearities and ultimately uncouple the dynamics, physical knowledge of the occurring effects during flight is required and needs to be modeled accurately. Although numerous approaches have been taken to enhance the resilience of NDI or to integrate it with adaptive control, NDI still necessitates an detailed model of the system. Furthermore, reliable measurements of the air data quantities are required to cover the occurring effects and estimate the current state vector.

Incremental [7, 8] and sensory NDI [6, 9, 10] address these issues by eliminating the dependence on the knowledge of the internal dynamics comprising the aerodynamic effects. Those control laws either use series expansion and linearize the dynamics or replace the internal dynamics with sensor measurements. On the drawback side, those approaches tend to increase the aggressiveness to disturbances [11] and to over-utilize the control surface actuators. However, both approaches mainly depend on inertial measurements and measured control surface deflections, except for estimating the control effectiveness. These are considered to be less prone to failures than air data sensors, or are at least independent of them..

Hybrid (incremental) NDI (hNDI) combines sensory (or incremental) NDI and NDI by using a complementary filter. Its functionality and motivation has already been demonstrated in [6, 12]. A hidden gem of the hybrid NDI control approach is its ability to cut off the dependence on NDI and thus the dependence on air data sensor measurements. We exploit this property to develop a new approach to control law degradation in the case of air data sensor failures, which allows the control law to be reduced without sacrificing handling qualities. Finally, its applicability is demonstrated in flight tests on a CS-25 aircraft.

2 Control Theory: Hybrid Nonlinear Dynamic Inversion

A non-linear non-affine state-space system of form

$$\dot{x} = f(x) + g(x, u) \tag{1a}$$

$$\begin{bmatrix} y_{\text{com}} \\ y_{\text{add}} \end{bmatrix} = h(x) \tag{1b}$$

is assumed, where x represents the state vector, u the input vector, y the output vector, $f(x)$ the *internal dynamics*, $g(x,u)$ the *input dynamics*, and $h(x)$ the *output dynamics*. Furthermore, we assume full-state observability and sufficient smoothness of $g(x,u)$ in u so that nonlinear equation solvers can be applied. The output is separated into the *commanded* part y_{com}, which will be the input of the inversion law, and additional sensor measurements y_{add}, which provide additional information and allow the reconstruction of the state vector.

Nonlinear Dynamic Inversion (NDI) inverts the plant dynamics to get the input u_{NDI} necessary to achieve a given virtual control input $\nu = \dot{y}_{\text{com}}$ by using an estimation of the state space function, $\hat{f}$ and $\hat{g}$, i.e., the on-board model. If $\dim u > \dim \nu$, then control allocation methods are required to solve the inversion problem [13]. "Hard-wiring" of combined control deflections is the most based approach (e.g. combined differential deflection of ailerons, or identical deflection of elevators).

In this case, it is assumed that $\dim u = \dim \nu$. Then, the NDI control law can be written as

$$\hat{g}\left(\hat{x}, u_{\text{NDI}}\right) = \nu - \hat{f}(\hat{x}) \implies u_{\text{NDI}} = \hat{g}^{-1}\left(\hat{x},\ \nu - \hat{f}(\hat{x})\right) \tag{2}$$

with estimated state vector $\hat{x}$ and the inverse function $\hat{g}(\hat{u}, \hat{g}^{-1}(\hat{x}, z)) = z$ for a bijective function $\hat{g}$.

2.1 Sensory and Incremental Nonlinear Dynamic Inversion

Sensory NDI (sNDI) approximates the estimated dynamics $\hat{f}(\hat{x})$ in (2) by sensor measurements of the state derivatives $\hat{\dot{x}}$ and inputs $\hat{u}$ as

$$\hat{f}(\hat{x}) \approx \hat{\dot{x}} - \hat{g}(\hat{x},\ \hat{u}) \tag{3}$$

By using this approximation, the NDI law becomes the sensory NDI law, i.e.,

$$\hat{g}\left(\hat{x},\ u_{\text{sNDI}}\right) = \nu - \hat{\dot{x}} + \hat{g}(\hat{x},\ \hat{u}) \tag{4}$$

which can be solved in multiple ways [13, 14] and is equal to the incremental NDI law for $\hat{g}(\hat{x}, u) = \hat{G}(\hat{x})u$ if $\hat{G}(\hat{x})$ is invertible, but allows for an absolute control command. One common way to solve (4) is by using an incremental approach, i.e., linearizing around the current state and input measurements by using the 1st Taylor polynomial and ignoring higher-order terms, as

$$\hat{g}\left(\hat{x},\ u\right) \approx \hat{g}\left(\hat{x}, \hat{u}\right) + \left.\frac{\partial \hat{g}(x,u)}{\partial u}\right|_{\substack{x=\hat{x} \\ u=\hat{u}}} (u - \hat{u}) \tag{5}$$

$$u \approx \left(\left.\frac{\partial \hat{g}(x,u)}{\partial u}\right|_{\substack{x=\hat{x} \\ u=\hat{u}}}\right)^{-1} \left(\nu - \hat{\dot{x}}\right) + \hat{u} \tag{6}$$

This is equal to the incremental NDI law, which is commonly derived by taking the Taylor expansion of an estimation of (1a) around (x_0, u_0) to the 1st Taylor polynomial and ignoring higher-order terms, yielding

$$\dot{x} \approx \underbrace{\hat{f}(x_0) + \hat{g}(x_0, u_0)}_{\dot{x}_0} + \left(\left.\frac{\partial \hat{g}(x,u)}{\partial x}\right|_{\substack{x=x_0 \\ u=u_0}} + \left.\frac{\partial \hat{f}(x)}{\partial x}\right|_{x=x_0}\right) \underbrace{(x - x_0)}_{\Delta x} + \left.\frac{\partial \hat{g}(x,u)}{\partial u}\right|_{\substack{x=x_0 \\ u=u_0}} \underbrace{(u - u_0)}_{\Delta u} \tag{7}$$

It is common practice to use the state and input measurements as an expansion point, i.e., $(x_0, u_0) = (\hat{x}, \hat{u})$, and approximating $\dot{x}_0$ by the measurement $\hat{\dot{x}}$. Furthermore, by applying the time scale separation principle

and assuming a slower or negligible state change Δx in comparison to faster control input changes Δu, i.e., $\Delta x \ll \Delta u$, we arrive at the incremental NDI law [7]

$$\Delta u_{\mathrm{iNDI}} = \left(\left. \frac{\partial g(x,u)}{\partial u} \right|_{\substack{x=x_0 \\ u=u_0}} \right)^{-1} \left(\nu - \hat{\dot{x}} \right) \tag{8}$$

In summary, the basic idea of sensory as well as incremental NDI is to replace the dependence on $\hat{f}$ with measurements of the state vector derivatives $\hat{\dot{x}}$ and the current input $\hat{u}$, according to (3), to achieve an inversion of the form

$$\hat{g}\left(\hat{x},\, u_{\mathrm{sNDI}}\right) = \nu - \hat{\dot{x}} + \hat{g}(\hat{x},\, \hat{u}) \tag{4}$$

$$\Delta u_{\mathrm{iNDI}} = \left(\left. \frac{\partial g(x,u)}{\partial u} \right|_{\substack{x=x_0 \\ u=u_0}} \right)^{-1} \left(\nu - \hat{\dot{x}} \right) \tag{8}$$

While (8) and (4) do not depend on $\hat{f}$, they are exposed to the measurements $\hat{\dot{x}}$ and $\hat{u}$, which need to be synchronized. Furthermore, both measurements have a direct link on the commanded control surface deflection u_{iNDI} or u_{sNDI}. These issues are well known [11, 12, 15]. However, the incremental nature of (8) requires control allocation algorithms to be applied on incremental inputs Δu instead of absolute inputs u, and is furthermore inherently discrete.

2.2 Hybrid Nonlinear Dynamic Inversion

Classical and sensory NDI have considerable advantages and disadvantages that, fortunately, are mostly complementary to each other. Sensory NDI provides excellent tracking performance with minimal use of sensor data (e.g., full state feedback is typically not required). However, it does not permit the trade of control activity against tracking performance, which may be advantageous in turbulent conditions or at frequencies where this is no longer feasible for comfort or flight load reasons [11]. Modeling errors may rapidly reduce the performance of NDI-based control laws. However, the method does accommodate the aforementioned trade-off. Hybrid NDI combines both methods and uses a complementary filter κ to combine NDI and sensory NDI, i.e., it combines the estimated internal dynamics from the NDI approach, $\hat{f}(\hat{x})$, with the estimated internal dynamics from the sensory NDI approach, $\hat{\dot{x}} - \hat{g}(\hat{x}, \hat{u})$, into a complementary filtered signal f_{compl}. In this way, we achieve the "best of both worlds": better performance at low frequencies due to sensor measurements and compensation for NDI model inaccuracies, and better performance at higher frequencies by favoring smooth NDI commands over noisy sensor measurements. Simultaneously, we can ensure that control surface commands of the sensory NDI are filtered appropriately.

The hybrid NDI law can be stated as

$$\hat{g}\left(\hat{x},\, u_{\mathrm{hNDI}}\right) = \nu - f_{\mathrm{compl}}\left(\hat{\dot{x}}, \hat{x}, \hat{u}\right) \tag{9}$$

A complementary filter of first order can be realized as shown in Fig. 1 where the NDI share $\hat{f}(\hat{x}) = f_h$ is being high-pass filtered and the sensory NDI share $\hat{\dot{x}} - \hat{g}(\hat{x}, \hat{u}) = f_l$ is being low-pass filtered, which yields the following relation

$$\kappa: \quad \frac{\mathrm{d}}{\mathrm{d}t} f_{\mathrm{compl}} = -K\, f_{\mathrm{compl}} + K f_l + \frac{\mathrm{d}}{\mathrm{d}t} f_h = -K f_{\mathrm{compl}} + K \cdot \left(\hat{\dot{x}} - \hat{g}(\hat{x}, \hat{u}) \right) + \frac{\mathrm{d}}{\mathrm{d}t} \hat{f}(\hat{x}) \tag{10}$$

Different implementations of the complementary filter are illustrated in Fig. 1. Fig. 1a shows an ideally implemented continuous-time complementary filter. Fig. 1b is the counterpart to the first, but

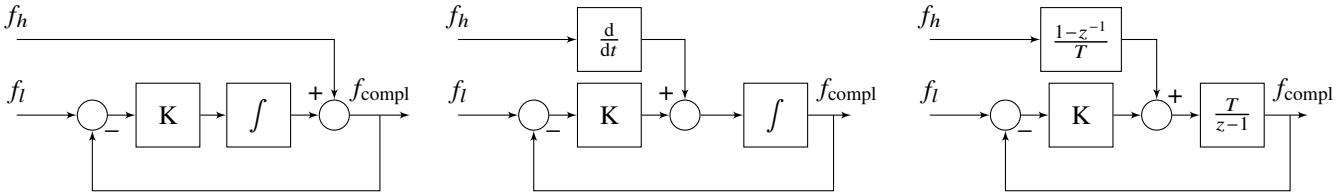

(a) Continuous-time **(b) Continuous-time with differentiation** **(c) Discrete-time version of (1b)**

Fig. 1 First-order complementary filter of high-pass f_h and low-pass f_l share.

with differentiation. Differentiating first and integrating afterward allows continuous switching without discontinuities, as well as resetting and initializing the filter appropriately. Fig. 1c shows the discretized filter using the forward integration method. This study does not consider more advanced implementations of discrete-time integrators and differentiators or higher-order complementary filter implementations. These could be used to further improve the implementations, but as demonstrated later, they are optional to achieve the basic functionality.

The final 1st order hybrid NDI law can thus be described by a stateful system

$$\frac{\mathrm{d}}{\mathrm{d}t} f_{\text{compl}} = -K\, f_{\text{compl}} + K \cdot \Big(\underbrace{\hat{x} - \hat{g}(\hat{x}, \hat{u})}_{f_l} \Big) + \frac{\mathrm{d}}{\mathrm{d}t} \underbrace{\hat{f}(\hat{x})}_{f_h} \tag{10}$$

$$\hat{g}\,(\hat{x},\, u_{\text{hNDI}}) = \nu - f_{\text{compl}} \tag{9}$$

3 Control Law Implementation and Air Data Sensor Failures

For fixed-wing aircraft attitude control, the angular rates equation of the equations of motion is inverted in the control law. This way, a relative degree of 1 and full determination are ensured. The angular rate equation is given as

$$\underbrace{\dot{\boldsymbol{\omega}}}_{\dot{x}} = \underbrace{\boldsymbol{I}^{-1} \left(\boldsymbol{m}^{\mathrm{B}} - \boldsymbol{\omega} \times \boldsymbol{I}\boldsymbol{\omega} \right)}_{f(x)} + \underbrace{\bar{q} S\, \boldsymbol{I}^{-1} \boldsymbol{C}_{\delta}}_{G(x)} \underbrace{\boldsymbol{\delta}_{\text{cs}}}_{u} \tag{11}$$

with the angular rates $\boldsymbol{\omega} = \begin{bmatrix} p & q & r \end{bmatrix}^T$, the moment of inertia $\boldsymbol{I}$, the total moments acting on the center of gravity in body frame $\boldsymbol{m}^{\mathrm{B}}$, the dynamic pressure $\bar{q} = \frac{1}{2}\rho V_{\mathrm{a}}^2$, the wing's reference area S, the control effectiveness matrix $\boldsymbol{C}_{\delta}$, and the control surface deflections $\boldsymbol{\delta}_{\text{cs}} = \begin{bmatrix} \delta_a & \delta_e & \delta_r \end{bmatrix}^T$ consisting of a single aileron, elevator, and rudder deflection. Note that (11) assumes a control-affine form, which (approximately) applies for the used model in Section 4. Furthermore, the inversion is fully determined by using combined control surfaces.

By neglecting other than aerodynamic influences on the acting total moments, i.e., neglecting propulsion and environmental moments, the hybrid NDI control law in (9) can be realized with

$$\hat{f}(\hat{x}) = \hat{\boldsymbol{I}}^{-1} \cdot \left(\hat{\bar{q}} S \cdot \begin{bmatrix} \frac{b}{2} \hat{C}_l \\ \bar{c}\, \hat{C}_m \\ \frac{b}{2} \hat{C}_n \end{bmatrix} - \hat{\omega} \times \hat{\boldsymbol{I}} \hat{\omega} \right) \tag{12}$$

$$\hat{G}(\hat{x}) = \hat{\bar{q}} S \hat{\boldsymbol{I}}^{-1} \underbrace{\begin{bmatrix} \frac{b}{2}\hat{C}_{l_{\delta a}} & 0 & \frac{b}{2}\hat{C}_{l_{\delta r}} \\ 0 & \bar{c}\,\hat{C}_{m_{\delta e}} & 0 \\ \frac{b}{2}\hat{C}_{n_{\delta a}} & 0 & \frac{b}{2}\hat{C}_{n_{\delta r}} \end{bmatrix}}_{\hat{\boldsymbol{C}}_\delta} \tag{13}$$

with the estimated aerodynamic roll moment coefficient $\hat{C}_l\,(V_\mathrm{a}, \alpha, \beta, \rho, \omega)$, pitch moment coefficient $\hat{C}_m\,(V_\mathrm{a}, \alpha, \beta, \rho, \omega)$, and yaw moment coefficient $\hat{C}_n\,(V_\mathrm{a}, \alpha, \beta, \rho, \omega)$, as well as the estimated control effectiveness coefficients in $\hat{\boldsymbol{C}}_\delta$. Then, the hybrid NDI law for (11) is

$$\delta_\mathrm{cs} = \frac{1}{\hat{\bar{q}} S} \hat{\boldsymbol{C}}_\delta^{-1}\, \hat{\boldsymbol{I}} \left(\nu_\omega - f_\mathrm{compl}\left(\hat{\dot{x}}, \hat{x}, \hat{u}\right) \right) \tag{14}$$

3.1 Degradation in case of failure

To show the effect of an air data sensor failure, it is sufficient to look at the complementary filter and its inputs, as shown in (10). The dependence on $\hat{G}(\hat{x})$ is inevitable. However, the NDI part depends on $\hat{f}(\hat{x})$, while the sensory NDI part depends on $\hat{\dot{x}}$ and $\hat{G}(\hat{x})\hat{u}$. Both NDI and sensory NDI use $\hat{G}(x)$, which depends less on air data measurements (actually, the significant influence on G is due to $\bar{q} \propto V^2$). However, velocity can be estimated inertially.

Sensory NDI relies mostly on inertial measurements and is therefore more robust to an air data sensor failure. As motivated earlier, the idea of failure handling with hybrid NDI is to switch off the NDI part and rely solely on the sensory NDI part. Seamless and smooth switching is necessary. This can be achieved by using a complementary filter design as shown in Fig. 2. By adding a switch to cut off the

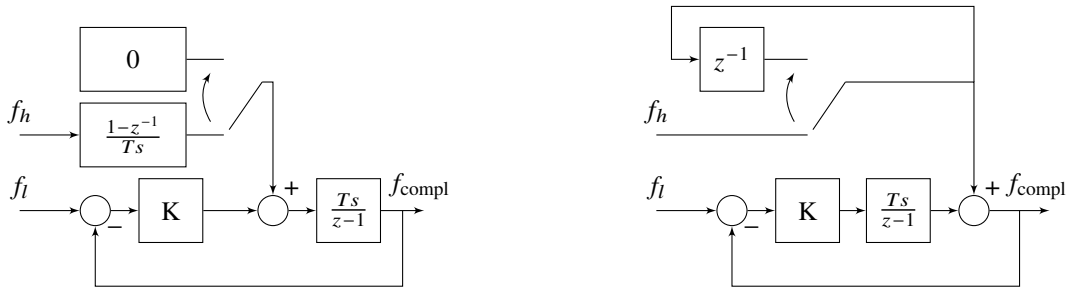

(a) Discrete-time filter with differentiation **(b) Discrete-time filter without differentiation**

Fig. 2 First-order complementary filter of high-pass f_h and low-pass f_l share with airdata failure mitigation.

NDI part, the hybrid NDI controller can operate solely as a filtered sensory NDI controller. The system turns off the NDI when an air data failure is detected. However, implementation-wise, it is crucial to avoid any discontinuities during switching. This is relevant because the output of the NDI controller is - more or less - directly commanded to the actuators. This can be achieved by using a filter implementation as shown in Fig. 2.

Sensitivity of the control law with respect to air data measurements ($\hat{\alpha}$, $\hat{\beta}$, $\hat{V}_\mathrm{a}$) can be estimated by looking at the gradient of the control command δ_cs, which yields

$$\frac{\partial \delta_\mathrm{cs}}{\partial \hat{\alpha}} = -\frac{1}{\hat{\bar{q}} S} \left(\hat{\boldsymbol{C}}_\delta^{-1}\, \hat{\boldsymbol{I}}\, \frac{\partial f_\mathrm{compl}}{\partial \hat{\alpha}} + \frac{\partial\, \hat{\boldsymbol{C}}_\delta^{-1}}{\partial \hat{\alpha}} \hat{\boldsymbol{I}} f_\mathrm{compl} \right) \approxeq -\frac{1}{\hat{\bar{q}} S} \hat{\boldsymbol{C}}_\delta^{-1}\, \hat{\boldsymbol{I}}\, \frac{\partial f_\mathrm{compl}}{\partial \hat{\alpha}} \tag{15}$$

$$\frac{\partial \delta_\mathrm{cs}}{\partial \hat{\beta}} = -\frac{1}{\hat{\bar{q}} S} \left(\hat{\boldsymbol{C}}_\delta^{-1}\, \hat{\boldsymbol{I}}\, \frac{\partial f_\mathrm{compl}}{\partial \hat{\beta}} + \frac{\partial\, \hat{\boldsymbol{C}}_\delta^{-1}}{\partial \hat{\beta}} \hat{\boldsymbol{I}} f_\mathrm{compl} \right) \approxeq -\frac{1}{\hat{\bar{q}} S} \hat{\boldsymbol{C}}_\delta^{-1}\, \hat{\boldsymbol{I}}\, \frac{\partial f_\mathrm{compl}}{\partial \hat{\beta}} \tag{16}$$

$$\frac{\partial \delta_{\mathrm{cs}}}{\partial \hat{V}_{\mathrm{a}}} = -\frac{1}{\hat{\bar{q}} S}\left(\hat{\boldsymbol{C}}_{\delta}^{-1}\,\hat{\boldsymbol{I}}\,\frac{\partial f_{\mathrm{compl}}}{\partial \hat{V}_{\mathrm{a}}} + \frac{\partial\,\hat{\boldsymbol{C}}_{\delta}^{-1}}{\partial \hat{V}_{\mathrm{a}}}\hat{\boldsymbol{I}} f_{\mathrm{compl}} - \frac{2}{V_{\mathrm{a}}}\hat{\boldsymbol{C}}_{\delta}^{-1}\,\hat{\boldsymbol{I}}\,f_{\mathrm{compl}}\right) \tag{17}$$
$$\approxeq -\frac{1}{\hat{\bar{q}} S}\left(\hat{\boldsymbol{C}}_{\delta}^{-1}\,\hat{\boldsymbol{I}}\,\frac{\partial f_{\mathrm{compl}}}{\partial \hat{V}_{\mathrm{a}}} - \frac{2}{V_{\mathrm{a}}}\hat{\boldsymbol{C}}_{\delta}^{-1}\,\hat{\boldsymbol{I}}\,f_{\mathrm{compl}}\right)$$

where the sign $\approxeq$ denotes simplifications according to the numerical flight dynamics model (Section 4). The complementary filtered signal f_{compl} is the main factor. It is a product of filtering the signals $\hat{f}(\hat{x})$ and $\hat{\omega} - \hat{G}(\hat{x})\,\hat{\delta}_{\mathrm{cs}}$. Thus, its sensitivity regarding air data measurements can be estimated via the sensitivity of both

$$\frac{\partial \hat{f}(\hat{x})}{\partial \hat{\alpha}} = \hat{\bar{q}} S \hat{\boldsymbol{I}}^{-1}\begin{bmatrix} \frac{b}{2}\frac{\partial}{\partial \hat{\alpha}}\hat{C}_l \\ \bar{c}\,\frac{\partial}{\partial \hat{\alpha}}\hat{C}_m \\ \frac{b}{2}\frac{\partial}{\partial \hat{\alpha}}\hat{C}_n \end{bmatrix} \approxeq \hat{\bar{q}} S \hat{\boldsymbol{I}}^{-1}\begin{bmatrix} 0 \\ \bar{c}\,\hat{C}_{m_\alpha} \\ 0 \end{bmatrix} \tag{18}$$

$$\frac{\partial \hat{f}(\hat{x})}{\partial \hat{\beta}} = \hat{\bar{q}} S \hat{\boldsymbol{I}}^{-1}\begin{bmatrix} \frac{b}{2}\frac{\partial}{\partial \hat{\beta}}\hat{C}_l \\ \bar{c}\,\frac{\partial}{\partial \hat{\beta}}\hat{C}_m \\ \frac{b}{2}\frac{\partial}{\partial \hat{\beta}}\hat{C}_n \end{bmatrix} \approxeq \hat{\bar{q}} S \hat{\boldsymbol{I}}^{-1}\begin{bmatrix} \frac{b}{2}\hat{C}_{l_\beta} \\ 0 \\ \frac{b}{2}\hat{C}_{n_\beta} \end{bmatrix} \tag{19}$$

$$\frac{\partial \hat{f}(\hat{x})}{\partial \hat{V}_{\mathrm{a}}} = \hat{\bar{q}} S \hat{\boldsymbol{I}}^{-1}\begin{bmatrix} \frac{b}{2}\frac{\partial}{\partial \hat{V}_{\mathrm{a}}}\hat{C}_l \\ \bar{c}\,\frac{\partial}{\partial \hat{V}_{\mathrm{a}}}\hat{C}_m \\ \frac{b}{2}\frac{\partial}{\partial \hat{V}_{\mathrm{a}}}\hat{C}_n \end{bmatrix} + \underbrace{\frac{\partial \hat{\bar{q}}}{\partial \hat{V}_{\mathrm{a}}}}_{\hat{\rho}\hat{V}_{\mathrm{a}}} S \hat{\boldsymbol{I}}^{-1}\begin{bmatrix} \frac{b}{2}\hat{C}_l \\ \bar{c}\,\hat{C}_m \\ \frac{b}{2}\hat{C}_n \end{bmatrix} \approxeq \frac{2}{\hat{V}_{\mathrm{a}}}\hat{\bar{q}} S \hat{\boldsymbol{I}}^{-1}\begin{bmatrix} \frac{b}{2}\hat{C}_l \\ \bar{c}\,\hat{C}_m \\ \frac{b}{2}\hat{C}_n \end{bmatrix} \tag{20}$$

and

$$\frac{\partial\left[\hat{\omega} - \hat{G}(\hat{x})\,\hat{\delta}_{\mathrm{cs}}\right]}{\partial \hat{\alpha}} = -\hat{\bar{q}} S\,\hat{\boldsymbol{I}}^{-1}\,\frac{\partial}{\partial \hat{\alpha}}\hat{\boldsymbol{C}}_{\delta}\,\hat{\delta}_{\mathrm{cs}} \approxeq -\hat{\bar{q}} S\,\hat{\boldsymbol{I}}^{-1}\begin{bmatrix} 0 \\ \bar{c}\,\frac{\partial}{\partial \hat{\alpha}}\hat{C}_{m_{\delta e}}\cdot\hat{\delta}_e \\ 0 \end{bmatrix} \approx \begin{bmatrix} 0 \\ 0 \\ 0 \end{bmatrix} \tag{21}$$

$$\frac{\partial\left[\hat{\omega} - \hat{G}(\hat{x})\,\hat{\delta}_{\mathrm{cs}}\right]}{\partial \hat{\beta}} = -\hat{\bar{q}} S\,\hat{\boldsymbol{I}}^{-1}\,\frac{\partial}{\partial \hat{\beta}}\hat{\boldsymbol{C}}_{\delta}\,\hat{\delta}_{\mathrm{cs}} \approxeq \begin{bmatrix} 0 \\ 0 \\ 0 \end{bmatrix} \tag{22}$$

$$\frac{\partial\left[\hat{\omega} - \hat{G}(\hat{x})\,\hat{\delta}_{\mathrm{cs}}\right]}{\partial \hat{V}_{\mathrm{a}}} = -\hat{\bar{q}} S\,\hat{\boldsymbol{I}}^{-1}\left(\frac{\partial}{\partial \hat{V}_{\mathrm{a}}}\hat{\boldsymbol{C}}_{\delta}\,\hat{\delta}_{\mathrm{cs}} + \frac{2}{\hat{V}_{\mathrm{a}}}\hat{\boldsymbol{C}}_{\delta}\,\hat{\delta}_{\mathrm{cs}}\right) \approxeq -\frac{2}{\hat{V}_{\mathrm{a}}}\,\hat{\bar{q}} S\,\hat{\boldsymbol{I}}^{-1}\hat{\boldsymbol{C}}_{\delta}\,\hat{\delta}_{\mathrm{cs}} \tag{23}$$

The results are of interest from a number of perspectives. Firstly, while $\hat{f}(\hat{x})$ is sensitive to inaccuracies (or the absence) of $\hat{\alpha}$ and $\hat{\beta}$, $\hat{\omega} - \hat{G}(\hat{x})\,\hat{\delta}_{\mathrm{cs}}$ is (approximately) not. Secondly, the sensitivity of both terms with regard to airspeed is approximately equal. This indicates that sensory NDI does not exhibit a significant advantage over NDI in terms of airspeed sensitivity. However, a third observation is that dynamic inversion in general, that is to say, sensory NDI and NDI, has only a small sensitivity regarding the airspeed. Although the terms do not vanish, they represent the nominal contribution of either the "internal" or "external" dynamics to the angular rate derivative, but are scaled by $\frac{2}{\hat{V}_{\mathrm{a}}}$, which makes it even less sensitive.

The analysis presented is preliminary work on this topic and requires further investigation and a more detailed analysis to fully elucidate its potential. Nevertheless, these findings already suggest that the sensory component, i.e., $\hat{\omega} - \hat{G}(\hat{x})\,\hat{\delta}_{\mathrm{cs}}$, is indeed relatively insensitive to air data measurement errors, particularly to $\hat{\alpha}$ and $\hat{\beta}$, in comparison to the NDI component, i.e., $\hat{f}(\hat{x})$. Nevertheless, both the sensory

part and the NDI part are found to be sensitive to the airspeed measurement $\hat{V}_a$ although only to a limited extent. This relation can also be observed in simulative experiments and the flight tests in Section 4.

4 Flight Test Results

The proposed controller feature for switching off the NDI part in case of air data failure has been tested on a CS-25 aircraft: the Cessna Citation II "PH-LAB" of the Technical University of Delft and the NLR. The *PH-LAB* research platform (see Fig. 3) is certified according to EASA CS-25 "Certification Specification for Large Aeroplanes" with an experimental fly-by-wire system [16]. The flight hardware is described in detail in [16–19]. A high-fidelity flight dynamics model is available for this aircraft. Furthermore, NDI and incremental NDI flight tests have already been conducted on the *PH-LAB* based on this model [17–19]. Thus, the *PH-LAB* model is an ideal basis for flight control law testing.

Fig. 3 Cessna Citation II (Model 550) Research Aircraft *PH-LAB*

We conducted two different tests, one using automatically generated commands and the other a *pilot-in-the-loop* test. To keep the complexity low, it is assumed that there is a system for detecting air data sensor failures that triggers the controller degradation. In this study, the air data sensor failure is triggered in software and results in a control law degradation that ignores the angle of attack and sideslip measurements and replaces the airspeed measurement with an estimate.

First, the general effects of switching were investigated by triggering an air data sensor failure and then looking at the degraded step response. The response of an 11° step in roll angle ϕ is shown in Fig. 4.

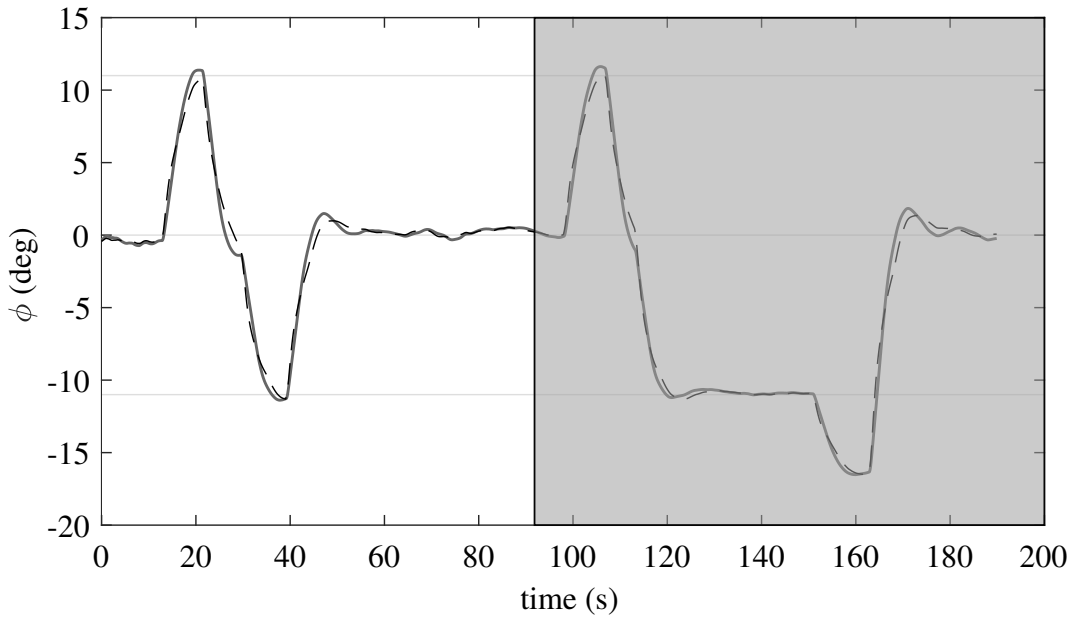

Fig. 4 Roll angle tracking with air data failure. Command (dashed) and measured value (gray). Grayed areas mark air data sensor failures.

In the second test, the experimental pilot operated the aircraft with the hybrid NDI controller enabled. Subsequently, air data sensor failures were randomly triggered without prior notification to the experimental pilot. The objective of this experiment was to provide a subjective indication of the

handling performance of the degraded controller. Fig. 5 depicts the recorded roll angle during this test. The experimental pilot was unable to discern any change in the aircraft's handling characteristics. The experiment was repeated with the other pilots and flight test crew members commanding the hybrid NDI controller, and similar results were obtained.

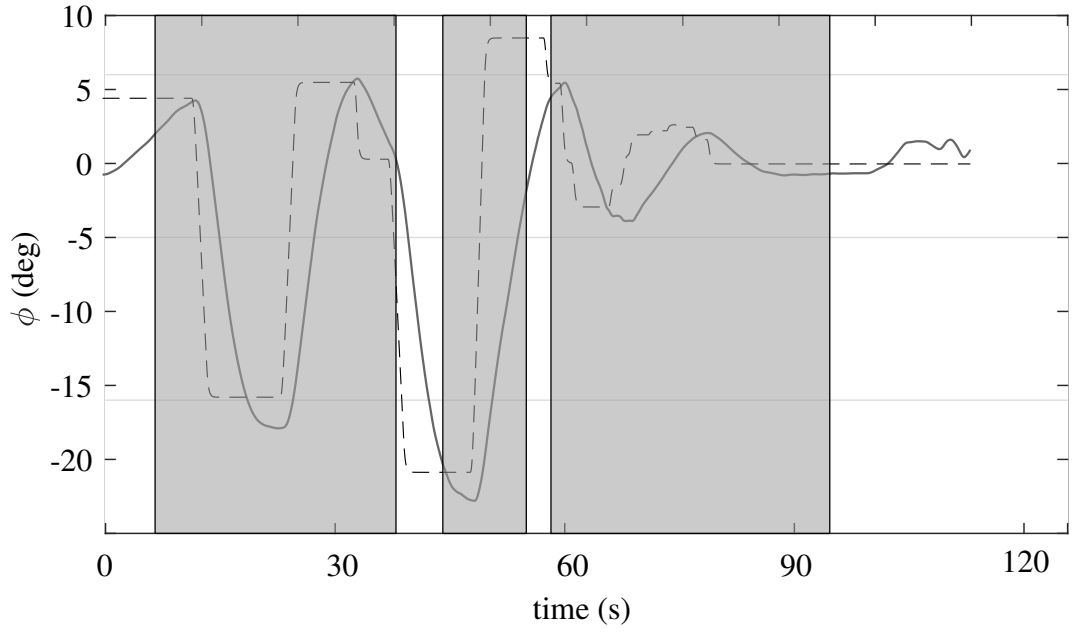

Fig. 5 Roll rate/angle tracking with pilot-in-the-loop and air data failure. Command (dashed) and measured value (gray). Grayed areas mark air data sensor failures

During the flight tests, the controller was degraded (switched) without any noticeable adverse effects. Additionally, no subjective differences in handling qualities were discernible. Although the experiment lacks statistical significance and did not cover the entire flight control function envelope, the results indicate that the developed solution to control law degradation in case of air data sensor failure is promising.

5 Conclusion

In the event of an air data sensor failure, pilots are placed in a highly stressful situation. Current control laws have the effect of increasing the workload of the pilot even more by reducing the level of automation of the flight control system, which in turn affects the handling behaviour of the aircraft. Hybrid NDI represents a promising control method that combines both NDI and sensory NDI via a complementary filter. Incorporating a cutoff switch into the complementary filter enables the degradation of the hybrid NDI law to a filtered sensory NDI law. This has the primary advantage of being comparatively independent of air data measurements, while exhibiting similar handling characteristics. Flight test results indicate that the proposed addition to the hybrid NDI controller for the cutoff of the air data-dependent part is a viable option for further investigation.

Acknowledgments

The authors would like to acknowledge the teams at DLR and TU Delft, without whose contributions the flight test campaign would not have been possible. Special thanks go to our colleague Christian Weiser, who helped with his flight control and flight test experiences. Additional thanks go to our partner from TU Delft, who provided the flight test framework and their expertise, including Menno Klaasen, Fred den Toom, Olaf Stroosma, René van Passen, and Ferdinand Postema. The authors want to especially

thank our test pilots, Alexander in't Velt and Hans Mulder, who showed patience, calm, and fun and provided us with a great and safe flight test experience.

References

[1] C. Favre. Fly-by-wire for commercial aircraft: the airbus experience. *International Journal of Control*, 59(1):139–157, 1994. DOI: 10.1080/00207179408923072.

[2] Pascal Traverse, Isabelle Lacaze, and Jean Souyris. Airbus fly-by-wire: A total approach to dependability. In Renè Jacquart, editor, *Building the Information Society*, pages 191–212, Boston, MA, 2004. Springer US. ISBN: 978-1-4020-8157-6.

[3] Daniel Ossmann and Hans-Dieter Joos. *Enhanced detection and isolation of angle of attack sensor faults*. 2016. DOI: 10.2514/6.2016-1135.

[4] Georges Hardier, Cédric Seren, and Pierre Ezerzere. Model–based techniques for virtual sensing of longitudinal flight parameters. *International Journal of Applied Mathematics and Computer Science*, 25(1):23–38, 2015. DOI: doi:10.1515/amcs-2015-0002.

[5] Daniel Ossmann and Hans-Dieter Joos. Combining sensor monitoring and fault tolerant control to maintain flight control system functionalities. *IFAC-PapersOnLine*, 49(17):46–51, 2016. ISSN: 2405-8963. 20th IFAC Symposium on Automatic Control in AerospaceACA 2016. DOI: https://doi.org/10.1016/j.ifacol.2016.09.009.

[6] Daniel Milz, Gertjan Looye, and Marc May. Dynamic inversion: An incrementally evolving methodology for flight control design. 2024. To be published.

[7] S. Sieberling, Q. P. Chu, and J. A. Mulder. Robust flight control using incremental nonlinear dynamic inversion and angular acceleration prediction. *Journal of Guidance, Control, and Dynamics*, 33(6):1732–1742, Nov. 2010. DOI: 10.2514/1.49978.

[8] Xuerui Wang, Erik-Jan van Kampen, Qiping Chu, and Peng Lu. Stability analysis for incremental nonlinear dynamic inversion control. *Journal of Guidance, Control, and Dynamics*, 42(5):1116–1129, May 2019. DOI: 10.2514/1.g003791.

[9] P. Smith. A simplified approach to nonlinear dynamic inversion based flight control. In *23rd Atmospheric Flight Mechanics Conference*. American Institute of Aeronautics and Astronautics, Aug. 1998. DOI: 10.2514/6.1998-4461.

[10] Barton Bacon and Aaron Ostroff. Reconfigurable flight control using nonlinear dynamic inversion with a special accelerometer implementation. In *AIAA Guidance, Navigation, and Control Conference and Exhibit*. American Institute of Aeronautics and Astronautics, Aug. 2000. DOI: 10.2514/6.2000-4565.

[11] Thiemo M. Kier, Reiko Müller, and Gertjan Looye. Analysis of automatic control function effects on vertical tail plane critical load conditions. In *AIAA Scitech 2020 Forum*. American Institute of Aeronautics and Astronautics, jan 2020. DOI: 10.2514/6.2020-1621.

[12] Yagiz Kumtepe, Tijmen Pollack, and Erik-Jan Van Kampen. Flight control law design using hybrid incremental nonlinear dynamic inversion. In *AIAA SCITECH 2022 Forum*. American Institute of Aeronautics and Astronautics, jan 2022. DOI: 10.2514/6.2022-1597.

[13] Daniel Milz, Marc Simon May, and Gertjan Looye. Dynamic inversion-based control concept for transformational tilt-wing evtols. In *AIAA SciTech 2024 Forum*, Januar 2024. DOI: 10.2514/6.2024-1290.

[14] Daniel Milz, Marc May, and Gertjan Looye. Tandem tilt-wing control design based on sensory nonlinear dynamic inversion. In *AIAA AVIATION 2024 Forum*, 2024.

[15] Rasmus Steffensen, Agnes Steinert, Zoe Mbikayi, Stefan Raab, Jorg Angelov, and Florian Holzapfel. Filter and sensor delay synchronization in incremental flight control laws. *Aerospace Systems*, jan 2023. DOI: 10.1007/s42401-022-00186-2.

[16] Peter Zaal, Daan Pool, Alexander in 't Veld, Ferdinand Postema, Max Mulder, Marinus van Paassen, and Jan Mulder. Design and certification of a fly-by-wire system with minimal impact on the original flight controls. In *AIAA Guidance, Navigation, and Control Conference*. American Institute of Aeronautics and Astronautics, jun 2009. DOI: 10.2514/6.2009-5985.

[17] Fabian Grondman, Gertjan Looye, Richard O. Kuchar, Q Ping Chu, and Erik-Jan Van Kampen. Design and flight testing of incremental nonlinear dynamic inversion-based control laws for a passenger aircraft. In *2018 AIAA Guidance, Navigation, and Control Conference*. American Institute of Aeronautics and Astronautics, jan 2018. DOI: 10.2514/6.2018-0385.

[18] Twan Keijzer, Gertjan Looye, Q Ping Chu, and Erik-Jan Van Kampen. Design and flight testing of incremental backstepping based control laws with angular accelerometer feedback. In *AIAA Scitech 2019 Forum*. American Institute of Aeronautics and Astronautics, jan 2019. DOI: 10.2514/6.2019-0129.

[19] Tijmen Pollack, Gertjan Looye, and Frans Van der Linden. Design and flight testing of flight control laws integrating incremental nonlinear dynamic inversion and servo current control. In *AIAA Scitech 2019 Forum*. American Institute of Aeronautics and Astronautics, jan 2019. DOI: 10.2514/6.2019-0130.